Flexible nano-ZnO/polyvinylidene difluoride piezoelectric composite films as energy harvester

Ritamay Bhunia[1] · **Shirsendu Das**[1] · **Saikat Dalui**[1,3] · **Shamima Hussain**[2] ·
Rajib Paul[1] · **Radhaballav Bhar**[1] · **Arun Kumar Pal**[1]

Abstract Nanogenerators (NGs) which harvest energy from mechanical vibration have attracted more attention in the past decade. Piezoelectric materials are the most promising candidates for developing NGs. Flexible free-standing nano-ZnO/PVDF composite films are prepared by incorporating different amounts of nano-ZnO fillers in PVDF matrix using sol–gel technique. Poled films show enhanced dielectric constant. The above free-standing films, with appropriate contacts, are subjected to energy harvesting studies. The output voltage increases with nano-ZnO loading in the PVDF matrix and shows enhanced effect for the poled films. Piezoelectric properties are investigated by measuring the piezoelectric charge constant (d_{33}) and piezoelectric voltage constant (g_{33}). A maximum AC output voltage ~ 4 V and output power of the order of few nanowatts are recorded for the nanogenerator which is used to light a red LED using a rectifying circuit through the discharging of a capacitor.

1 Introduction

Piezoelectric power generators emerged as a promising miniaturized power packages and self-powering of nanorobot and body-implanted device applications [1]. Despite

✉ Arun Kumar Pal
  msakp2002@yahoo.co.in

1   Department of Instrumentation Science, USIC Building, Jadavpur University, Calcutta 700 032, India

2   UGC-DAE CSR, Kalpakkam Node, Kokilamedu 603 104, India

3   Department of Physics, Sonamukhi College, Bankura 722 207, India

advancement in recent years, development of a direct current (DC) output nanogenerator (NG) remains very crucial for piezoelectric energy harvesting. In the past few years, self-powered devices have created a huge technological impact on smart and portable nanoelectronic applications. These self-powered devices help in reducing the device size further and subsequently improving their lifetime without battery [2]. The energy harvesting from human body movement has created enormous interest in the scientific world because of its ease of availability, cheap cost and independence of the environmental factors [3]. The self-powered operation is generally achieved by the integration of an energy harvester with the electronic devices. However, only a few studies have reported the successful generation of DC output power from nanogenerators. Park et al. [4] deposited $BaTiO_3$ thin films by radio frequency magnetron sputtering on a Pt/Ti/SiO$_2$/(100) Si substrate. The metal–insulator (poled-$BaTiO_3$)–metal-structured ribbons were successfully transferred onto a flexible substrate to form the NG structure. The above flexible $BaTiO_3$ nanogenerator generated an output voltage of up to 1.0 V. Recently, Lin et al. [5] also used $BaTiO_3$ nanotubes as piezomaterial prepared by hydrothermal method, and a composite of the above nanotubes with polymer poly(dimethylsiloxane) (PDMS) was made to fabricate NGs. Negligible signals for the device using unpoled samples were observed. Compared to the fabrication of $BaTiO_3$-based NG, reports on ZnO-based NG are not very many. Zhu et al. [6] reported the fabrication of high-output flexible nanogenerators using a sweeping-printing method. They managed to transfer vertically grown ZnO NWs to a flexible substrate and achieved horizontally aligned NW. The electrical output of the NG reached a peak voltage of 2.03 V and current of 107 nA. Because most piezoelectric NGs generate alternating

current (AC)-type charge output, the conversion of the signal from AC to DC requires a rectification circuit. This has a possibility of increasing the total size of the power package and degrades its power [7]. Nonetheless, requirement of efficient, smart, flexible and free-standing piezomaterial for the nanogenerator applications is still in great demand scientifically and technologically.

In this communication, we report here an easy, reproducible, cost-effective and scalable technique for depositing flexible free-standing nano-ZnO/PVDF composite films. The semicrystalline polymer, PVDF, is endowed with extraordinary piezoelectric, pyroelectric and dielectric properties [8, 9]. The β-phase controls its piezoelectric and pyroelectric properties. For that reason we chose this polymer for the ceramic-polymer composite. The possible utilization of the above flexible free-standing nano-ZnO/PVDF composite films as NG with improved performance for energy harvesting applications has been demonstrated. The films being flexible and free-standing will have an edge over other NG materials used so far.

2 Experimental

The following steps were involved in the synthesis of composite films of nano-ZnO/PVDF with three different amounts of nano-ZnO as filler in the PVDF matrix:
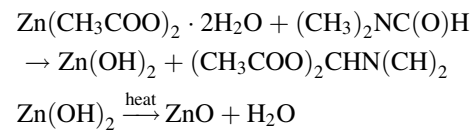
Step I: A stock solution (A) was prepared by taking 0.669 g of PVDF powder (Sigma-Aldrich) in a conical flask. Four milliliters of dimethyl formamide (DMF) was added to the above PVDF to make 15 wt% solution of PVDF with DMF, and the mixture was refluxed for 5–6 h with constant stirring at 60 °C for complete dissolution of the PVDF. Three such identical solutions were prepared in three different conical flasks.

Step II: Stock solutions (B) were prepared by taking three different amounts (26.34, 87.8 and 175.6 mg) of Zn acetate in three separate conical flasks. Four milliliters of DMF was added to each of these conical flasks. The solutions were refluxed for 1 h with constant stirring at room temperature (30 °C) for complete dissolution of the Zn acetate to obtain 0.03, 0.1 and 0.2 M solution of Zn acetate.

Step III: The temperatures of the individual stock solutions (B) were raised to 120 °C with continued refluxing and stirring for 3 h. The color of the mixture turned whitish, indicating the formation of $Zn(OH)_2$.

Step IV: 10–12 drops of diethanolamine was added to each of the above mixture. Diethanolamine would act as particle size controlling agent and an oxygen diffusion catalyst as well [10]. The temperature was further raised to 150 °C with continued stirring and refluxing for another 1 h till the solution became clear, indicating the formation of ZnO. The chemical reaction would follow the following path [11]:

$$Zn(CH_3COO)_2 \cdot 2H_2O + (CH_3)_2NC(O)H$$
$$\rightarrow Zn(OH)_2 + (CH_3COO)_2CHN(CH)_2$$

$$Zn(OH)_2 \xrightarrow{\text{heat}} ZnO + H_2O$$

Step V: One of the stock solutions (A) was poured in one of the above conical flasks containing ZnO as obtained in Step IV. The temperature was then decreased and fixed at 60 °C with continued stirring and refluxing for another 3 h when a clear gel was obtained.

Step V was repeated with the other two stock solutions as obtained in Step IV containing different amounts of ZnO to obtain appropriate gel for casting nano-ZnO/PVDF composite films containing three different amounts of ZnO.

The gels, thus obtained, were spin-casted uniformly on glass substrates at room temperature at a low spin (60 rpm) for depositing the nano-ZnO/PVDF composite films. A microwave oven was used to heat the as-coated films at 100 W for 3 min (temperature generated was ∼95 °C). The films so obtained could be easily peeled out from the glass substrate. The flexible free-standing films, thus obtained, were used for characterizations. We have avoided the conventional hot plate heating of the as-deposited spincast films to avoid pores arising out of bubbles emanating from the substrate/film interface. The low thermal conductivity of glass substrates would prevent homogeneous heating of the as-cast films, and hence, the glass/film interface would get heated before the heat could be transmitted uniformly throughout the film volume. This uneven heating associated with the hot plate heating was completely eliminated by microwave heating which imparted uniform heating throughout the bulk of the film. The quality of the films so obtained was extremely good, and the process was completely reproducible. The thicknesses of the composite films were ∼10 μm, and the active film area was ∼5 mm × 5 mm.

The films were poled in vacuum (∼10^{-6} Torr) at a field of 5 MV/m for 2 h. A schematic diagram of the poling unit is shown in Fig. 1a. The poling unit essentially consisted of a spring loaded electrode and a film holder acting as the second electrode. The above assembly was housed in a Pyrex glass vacuum chamber which could be evacuated to a level of ∼10^{-6} Torr. Appropriate feed-through allowed the high tension (HT) connections to be attached to the electrodes. The electrodes were connected to a regulated DC power supply (0–10 kV at 50 mA) with appropriate protection for short circuit.

A Carl Zeiss AURIGA field emission scanning electron microscopy (FESEM) was used to record the surface morphology at an operating voltage of 3 kV in secondary emission mode. Raman spectra were recorded using
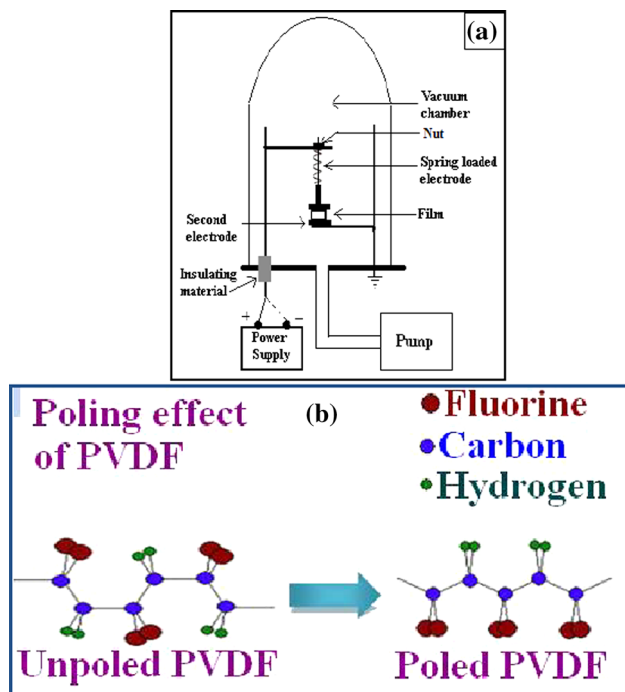
Fig. 1 a Schematic diagram of poling unit used and **b** schematic diagram of unpoled and poled PVDF

Renishaw inVia micro-Raman spectrometer. The spectra were collected at room temperature in line-focus mode using an eyepiece of 50X magnification, 785-nm laser (50 % power for PVDF films and at 1 % laser power for ZnO–PVDF films). High fluorescence generated due to the presence of ZnO nanocrystallites prevented use of higher laser power. Impedance data were recorded using a HIOKI 3532-50 LCR HiTESTER. The open-circuit piezoelectric voltage was measured by a mixed signal oscilloscope (YOKOGAWA-DLM 2004).

3 Results and discussion

3.1 Microstructural studies

The FESEM pictures of poled pristine PVDF film along with those for nano-ZnO/PVDF composite films with three different ZnO loadings are shown in Fig. 2a–d, respectively. The insets of above pictures depict the morphology of the corresponding unpoled ones. Changes in morphology of the PVDF films after nano-ZnO inclusion are apparent from the above micrographs (Fig. 2b–d). The texture of the films changed from near featureless (inset of Fig. 2a) to semifibrous natured one with the inclusion of nanocrystalline ZnO in the PVDF matrix (insets of Fig. 2b–d). The ZnO nanocrystallites are randomly dispersed with some aligned parallel to the surface resembling

fibrous structure. On poling, one surface of the host PVDF matrix would preferentially be fluorine-terminated while the other surface would be hydrogen-terminated (Fig. 1b) resulting in alignment of the dipoles. This would culminate in the generation of a strong electric field within the host PVDF matrix. The embedded ZnO nanocrystallites would also experience this field and would tend to orient themselves in the preferred c-axis orientation across the thickness of the PVDF film. This is reflected in the texture of the poled samples (Fig. 2b–d). Figure 2e shows a magnified picture for composite film with 0.2 M ZnO showing ZnO nanocrystallites. It may be observed that the crystallite sizes varied between 5 and 8 nm.

3.2 Raman studies

Raman spectra for a representative unpoled pristine PVDF in the range of 100–1600 cm^{-1} are shown in Fig. 3a. The spectra are dominated by moderate-to-strong characteristic peaks of various phases of PVDF located at $\sim$286 (α-phase), 410 (α-phase), 610 (α-phase), 797 (α-phase), 841 (β-phase), 875 (β-phase), 1146 (combination of α- and β-phases) and 1429 cm^{-1} (α-phase). Observations of the above peaks are in conformity with those reported by Constantino et al. [12] and Satpathy et al. [13]. The strong peak appearing at 797 cm^{-1} indicates that the major contribution in the film is of the TG (trans–gauche) sequence. The intrinsically weak band located at $\sim$841 cm^{-1} indicates the presence of trans–gauche–gauche–gauche (T3G) sequences. This band being common to both β- and γ-phases of PVDF would confirm the presence of either γ, β or both the phases in PVDF film. This observation is in conformity also with the studies reported by Boccaccio et al. [14]. The broad low intensity peak (Fig. 3a) appearing at $\sim$1146 cm^{-1} may be assigned to both the α- and β-phases present in PVDF films [12, 15]. The CH_2 bending mode appearing $\sim$1429 cm^{-1} was present in all the films studied here.

The modulation of Raman spectra with the addition of nanocrystalline ZnO in the PVDF matrix is depicted for the unpoled nano-ZnO/PVDF composite film in Fig. 3b, while those for the poled nano-ZnO/PVDF composite film recorded from hydrogenated- and fluorine-terminated surfaces are shown in Fig. 3c, d, respectively. It may be observed that all the above spectra contained signature peaks for PVDF as shown in Fig. 3a. The bands at 535 cm^{-1} can be attributed to CF_2 bending vibration, and the higher frequency band at $\sim$841 cm^{-1} may be due to out-of-phase combination of CH_2 rocking and CF_2 stretching mode (Fig. 3c, d) [16, 17]. These bands are mainly due to the presence of predominant β-phase [18]. The intensity of Raman peak for CH_2 modes was higher compared to that for CF_2 when recorded from hydrogen
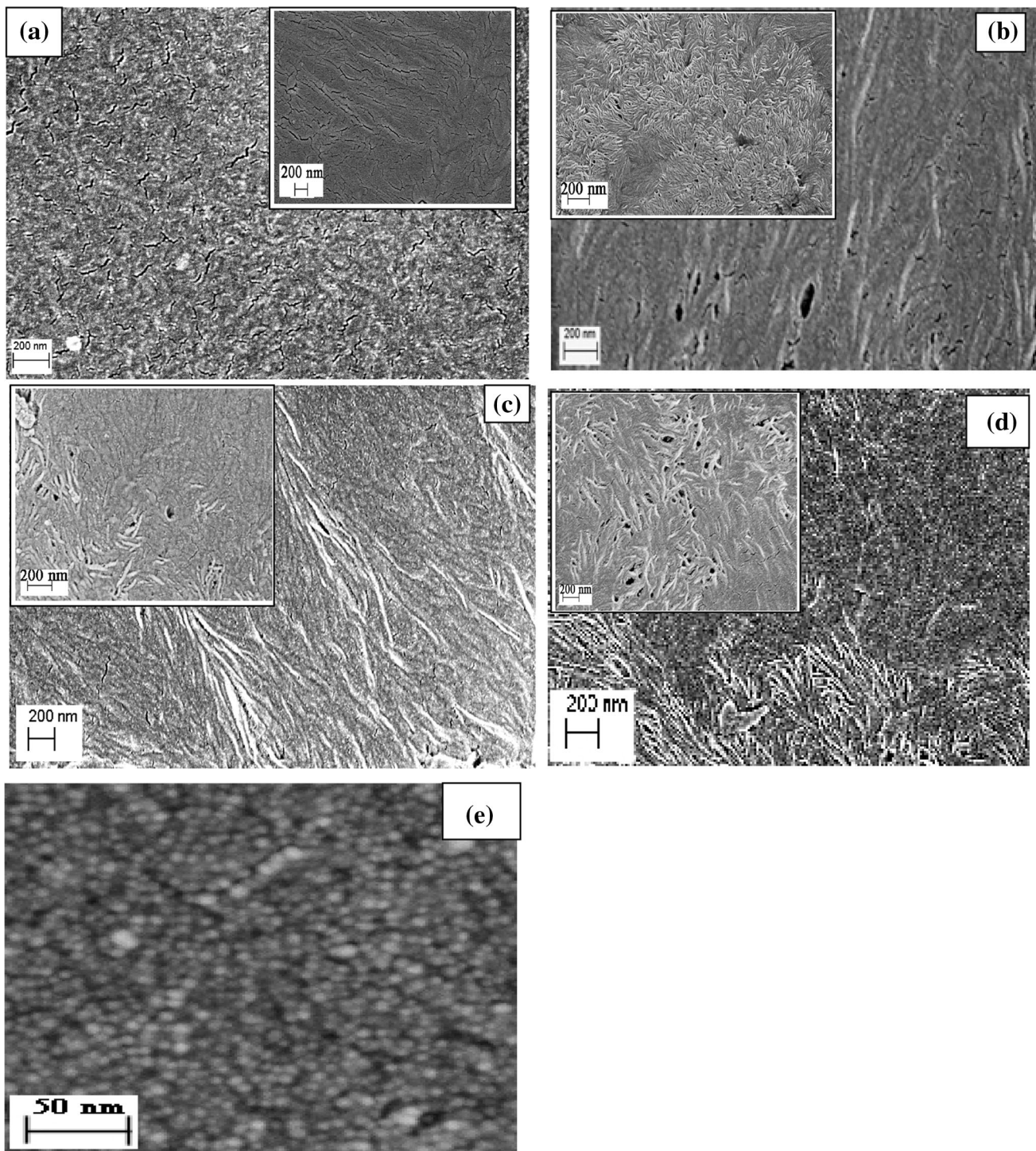
Fig. 2 FESEM pictures of: **a** poled pristine PVDF and three representative poled nano-ZnO/PVDF composite films samples with: **b** 0.03 M ZnO loading, **c** 0.1 M ZnO loading, **d** 0.2 M ZnO loading. *Insets* of (**a**), (**b**), (**c**) and (**d**) show the corresponding FESEM pictures of unpoled samples and (**e**) magnified image of the morphology of poled nano-ZnO/PVDF composite films with 0.2 M ZnO loading

(Fig. 3c)- and fluorine-terminated surface (Fig. 3b) and vice versa.

Besides the appearance of fingerprint peaks originating from PVDF host matrix, peaks related to ZnO nanocrystals could also be observed. As the amount of the filler (nano-ZnO) in PVDF matrix was quite low, the intensities of the peaks related to ZnO were also quite low. The peaks ~ 360 (Fig. 3b) and ~ 413 cm^{-1} (Fig. 3b) could be assigned to
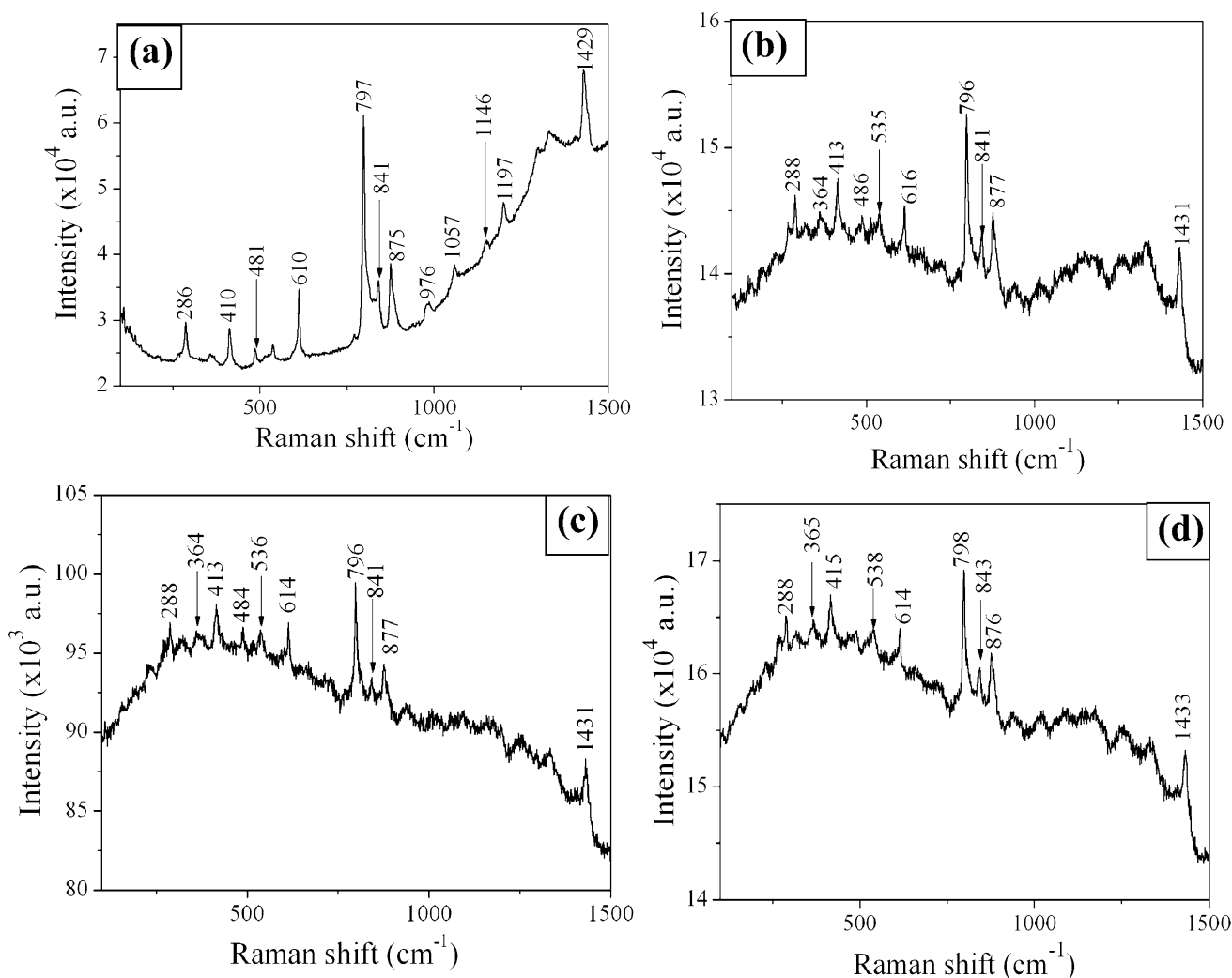
Fig. 3 Raman spectra of representative: **a** pristine PVDF film, **b** unpoled nano-ZnO/PVDF composite film, **c** poled nano-ZnO/PVDF composite films with 0.2 M ZnO loading recorded from hydrogen-terminated side and **d** poled nano-ZnO/PVDF composite films with 0.2 M ZnO loading recorded from fluorine-terminated side

the high frequency branch of E_2 mode of ZnO, which was the strongest mode in wurtzite crystal structure. The peak ~ 536 cm^{-1} could be assigned to A1 longitudinal optical (LO) mode of ZnO. The low intensity peak at ~ 283 cm^{-1} which overlapped with that for α-phase PVDF might have originated from the zone-boundary phonons of 2-E2(M) for ZnO. According to Kaschner et al. [19], Cheng et al. [20] and Bundesmann et al. [21], this mode was induced by host lattice defects, such as oxygen vacancies and Zn interstitials. It would be prudent to compare the modulation of Raman peaks due to inclusion of nano-ZnO in PVDF matrix. A huge background arising due to fluorescence of the ZnO nanocrystallites was observed in all the nano-ZnO/PVDF composite films. This background increased with increased laser power and was absent in the spectra of pristine PVDF films (Fig. 3a). This feature made normalization of the spectra difficult, and as such we refrained

from presenting the Raman data in normalized condition apprehending loss of information that would be revealed in the as-recorded spectra.

3.3 Impedance spectroscopy

It will be prudent to examine the modulation of frequency dispersion or dielectric relaxation of PVDF film with the inclusion of nano-ZnO in it. Collective response of microscopic polarization process under an external alternating electric field would be reflected from impedance analysis. Frequency dispersion or dielectric relaxation would be observed due to different polarization mechanisms present within a dielectric material. For impedance measurement, silver was evaporated using appropriate stainless steel mask from molybdenum boat on both the sides of the samples for contact. System pressure during

deposition was $\sim 10^{-6}$ Torr. The thicknesses of the composite films were ~ 10 μm, and the active contact area was ~ 5 mm $\times$ 5 mm for measurement. The frequency range was 1–100 kHz, and the amplitude of measuring AC field was 2 V. Variations of dielectric constant of unpoled and

poled PVDF film deposited here are shown in Fig. 4a. The dielectric constant was evaluated using the following relation,
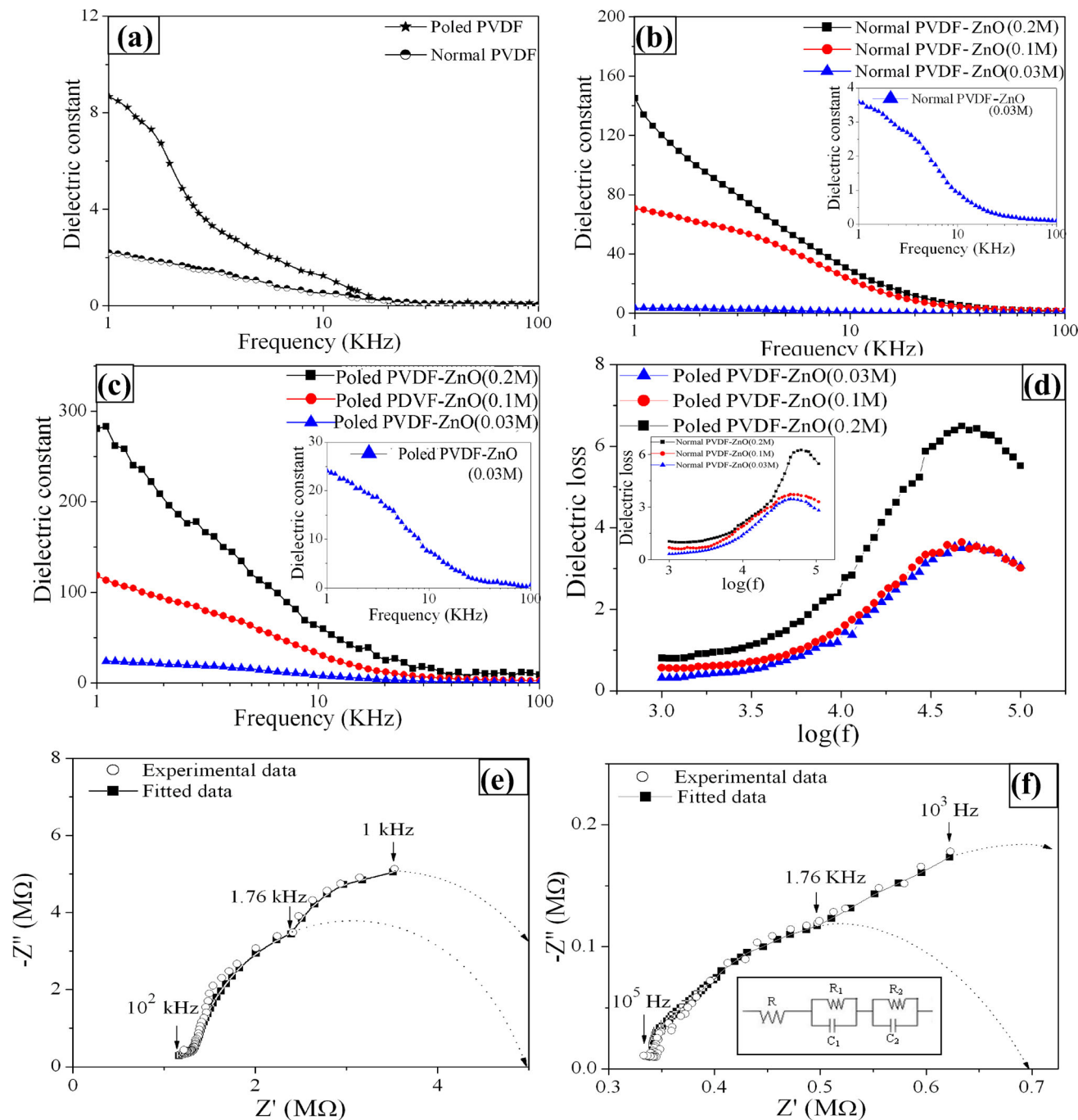
$$\varepsilon_r = \frac{Cd}{A\varepsilon_0} \qquad (1)$$

Fig. 4 Dielectric constant versus frequency plots: a unpoled and poled pristine PVDF film, b as-deposited unpoled nano-ZnO/PVDF composite films, c poled nano-ZnO/PVDF composite films. d Dielectric loss with different frequencies of poled nano-ZnO/PVDF films (*inset* shows the same for unpoled nano-ZnO/PVDF films).

e Experimental and theoretically fitted data points with the equivalent electrical circuit model of Cole–Cole plots for (b) representative unpoled nano-ZnO/PVDF composite film and f poled nano-ZnO/PVDF composite film

where d is the thickness of the sample, A is the area of the measured sample, and ε_0 is the free space permittivity. It could be observed that the dielectric constant increased significantly when the PVDF films were poled. The dielectric constants decreased rapidly with increasing frequency for the poled samples as compared to that for the unpoled samples. This rapid fall of dielectric constant (ε_1) with increased frequency indicates the significant contribution of space charge polarization to the total polarization observed in the poled films. Space charge polarization (interfacial polarization) would arise whenever phases of different conductivities are present in the same material. Thus, in the presence of an electric field, the charges would move through a conducting phase but would be interrupted as they come across a high resistivity phase. This would lead to a built-up of charge at the interface, which would manifest as enhanced polarization. These built-up charges cannot follow the applied field rapidly at high frequencies and hence the resultant loss. The dielectric constant value of the pristine PVDF film did not show significant change upon poling (Fig. 4a). But a significant increase (more than 10 times) in the dielectric constant of the films could be observed (Fig. 4b) with the inclusion of nano-ZnO in the PVDF matrix. Further, a 30 times increment in dielectric constant value was observed when the same films were poled (Fig. 4c). This is basically due to the alignment of ZnO nanocrystals in the PVDF host matrix upon poling, which has been substantiated from Raman studies (discussed in earlier section). One may argue at this point that since the electric field applied is mainly located in the PVDF and considering the ratio of the dielectric constant of PVDF over ZnO, then the electric force applied on the ZnO nanocrystals would be weak. This would imply that the force needed to align the ZnO crystals embedded in the PVDF matrix should be very strong. In this study, an electric field of 5 MV/m was applied for poling the ZnO/PVDF composite films which may facilitate the possible alignment of ZnO nanocrystallites in the PVDF matrix. At this juncture, it will be prudent to indicate that a conclusive proof of the suggested alignment of ZnO nanocrystallites in the PVDF matrix could be obtained from NMR measurement for direct observation of dipolar coupling. Also, at least supporting evidence could also be presented from TEM studies. Due to the lack of such instruments (NMR Bruker DXR spectrometer and HRTEM) for the above study, we refrained ourselves from making any conclusive comment on the alignment of ZnO nanocrystallites in PVDF matrix. It may also be noted here that we applied 5 MV/m for poling the ZnO/PVDF composite films which is also on higher side to ensure possible alignment of ZnO nanocrystallites in the PVDF matrix.

This would imply that poled nano-ZnO/PVDF composite free-standing flexible films would be an ideal material for energy harvesting applications with superior film properties. Table 1 shows the values of dielectric constant of different samples at 1 and 10 kHz.

The variation of the dielectric loss ($\tan(\delta) = -Z'/Z''$) with frequencies ($\log f$) for the poled and unpoled nano-ZnO/PVDF composite films is shown in Fig. 4d and the inset of Fig. 4d, respectively [22]. One may observed that the dielectric loss is low in the lower frequency range. The loss increases sharply with increase in frequency with the loss peaking at $\sim$48–50 kHz for both unpoled and poled samples. Nature of the above variation is similar that would be expected for a normal dielectric material. The higher values of dielectric constant and the lower values of dielectric loss at lower frequencies may originate due to contribution from all the three types of polarizations, viz space charge, dipole and electronic polarization. But at higher frequencies, significant contributions would arise only from the dipole and electronic polarizations. The observed high value of dielectric constant at low frequencies could be attributed to the interfacial polarization of dipoles arising out of localized motion of ZnO nanocrystals within the PVDF matrix. The decrease of dielectric constant and increase of dielectric loss with increasing frequency would mean a decrease in the response from the nano-ZnO dipoles. With the increase in frequency the dipoles would not be able to match up to the fast variation of the applied field and hence would result in a decreased response.

The unpoled and poled nano-ZnO/PVDF composite films were subjected to measurements of real and complex impedance as a function of test frequency. The data were recorded in the frequency range of 10^3–10^5 Hz. Plots Z' versus Z'' in complex plane for representative unpoled and poled nano-ZnO/PVDF composite films are shown in Fig. 4e, f, respectively. The above variation was nearly identical for all the nano-ZnO/PVDF composite films.

Appropriate equivalent circuit has to be identified so that it may represent the observed electrical properties of a sample. This would simplify the characterization of the properties of the devices under study. Generally, more than one circuit is required to represent a particular impedance spectrum of a composite material. Thus, the choice of appropriate equivalent circuit to describe such a system may pose a problem. Further, absence of well-accepted criteria to decide on the circuits that would be most appropriate in describing the impedance behavior would add up to the problem [23].

The Cole–Cole plot obtained for the nano-ZnO/PVDF composite films under study consisted of two superimposed

Table 1 Values of dielectric constants at 1 and 10 kHz

Sample	PVDF (g) in 4 ml DMF	Zn acetate (molar solution)	Dielectric constant			
			At 1 kHz		At 10 kHz	
			Normal film	Poled film	Normal film	Poled film
PVDF	0.669	0	2.19	8.67	0.52	1.25
ZnO/PVDF-1	0.669	0.03	3.59	22.37	0.94	12.07
ZnO/PVDF-2	0.669	0.1	70.75	119.41	22.82	32.67
ZnO/PVDF-3	0.669	0.2	144.71	281.24	29.78	63.55

semicircles. A simple model represented by $[R(R_1C_1)(R_2C_2)]$ which consists of a resistor R in series with one system R_1C_1 (resistance parallel with capacitor) in series with a second system R_2C_2 (resistance R_2 parallel with capacitor C_2) may be tried as a viable model to represent the observed behavior. The presence of two types of polarization may be represented by this model. Experimental and theoretically fitted data points, computed utilizing the above proposed model, are shown in Fig. 4e, f. The Cole–Cole plots of a representative nano-ZnO/PVDF composite film for an unpoled film (Fig. 4e) and a poled film (Fig. 4f) could be seen to be described well by the above proposed model. The starting frequency of the deviation from one semicircle arc to another one is at $\sim 1.76 \times 10^3$ Hz for these types of samples.

Now, the total impedance Z of the equivalent circuit can be described by the following equations:

$$Z = R + \frac{R_1/j\omega\ C_1}{R_1 + 1/j\omega C_1} + \frac{R_2/j\omega\ C_2}{R_2 + 1/j\omega C_2} \qquad (2)$$

The subscript of parameters refers to the element number in the proposed model circuits. The real and imaginary parts of Z may be separated as:

$$Z = Z' + jZ'' \qquad (3)$$

Z' and Z'' are the real and imaginary parts of the impedance, respectively.

R and C, as appeared in Eq. (2), denote the resistance and the capacitance, respectively; $j = \sqrt{-1}$; $\omega = 2\pi f$; f is the linear frequency. This model is basically a series model, and the total impedance (Z) could be expressed as $Z = Z' + jZ''$. Here, Z' and Z'' may be expressed as:

$$Z' = R_{eq} \qquad (4)$$

$$Z'' = -(1/\omega C_{eq}). \qquad (5)$$

where R_{eq} and C_{eq} are the equivalent resistance and the equivalent capacitance of the circuit, respectively. The dielectric loss (tan (δ)) of this series circuit now could be expressed as [22]:

$$\tan(\delta) = -Z'/Z'' = 2\pi f R_{eq} C_{eq} \qquad (6)$$

The equivalent capacitance would represent the capacitance measured at various frequencies during measurement. The resistance element (R) contained in this proposed circuit would dominate the impedance at high frequencies. The values of different parameters computed from the best fit of the proposed model are shown in Table 2. It may be noted that C_1 and C_2 values were significantly higher for poled PVDF/ZnO composite films. The dielectric constant also showed a significant increase for poled samples resulting in a significant increase in time constant for poled samples. The observed large decrease in device resistance upon poling could be ascribed to the proper alignment of the piezoelectric diploes in PVDF/ZnO composite films.

3.4 Energy harvesting studies

The above nano-ZnO/PVDF composite free-standing flexible films were subjected to energy harvesting studies. Silver contacts (5 mm diameter) were deposited on both sides of the films by evaporating silver from a conventional vacuum coating unit at a base vacuum $\sim 10^{-6}$ Torr. These films were then mounted on the experimental jig between two insulating clamps. Intermittent strain was generated by using different loads attached to the hammer striking the film (Fig. 5a, b). The output voltage was recorded using a memory oscilloscope. A bridge rectifier was used to rectify the input AC signal, and a 100-µF capacitor was connected to the output of the rectifier to store the charge. By the repetitive hammering, a capacitor could be charged up to ~ 4 V and a red LED could be lit using the discharging path of the capacitor.

Figure 6a shows the output voltage recorded for a pristine PVDF films, while Fig. 6b shows the output voltage signal of the same film when poled. One may observe the increase in the output voltage (doubled) upon poling. Interestingly, a 10 times increase in the output voltage was observed with the inclusion of nano-ZnO in the PVDF

Table 2 Parameters of the model circuit fitted to electrical impedance spectra for the PVDF–ZnO films

Sample	R (MΩ)	R_1 (MΩ)	R_2 (MΩ)	C_1 (pF)	C_2 (pF)	$R_1 C_1$ (ms)	$R_2 C_2$ (ms)
Unpoled PVDF/ZnO-1	0.99	13.92	0.35	25.9	9.29	0.36	0.003
Poled PVDF/ZnO-1	0.33	0.79	0.28	258	53.1	0.203	0.015

Fig. 5 **a** Schematic diagram of energy harvesting experimental setup, **b** real-time picture of the energy harvesting experiment
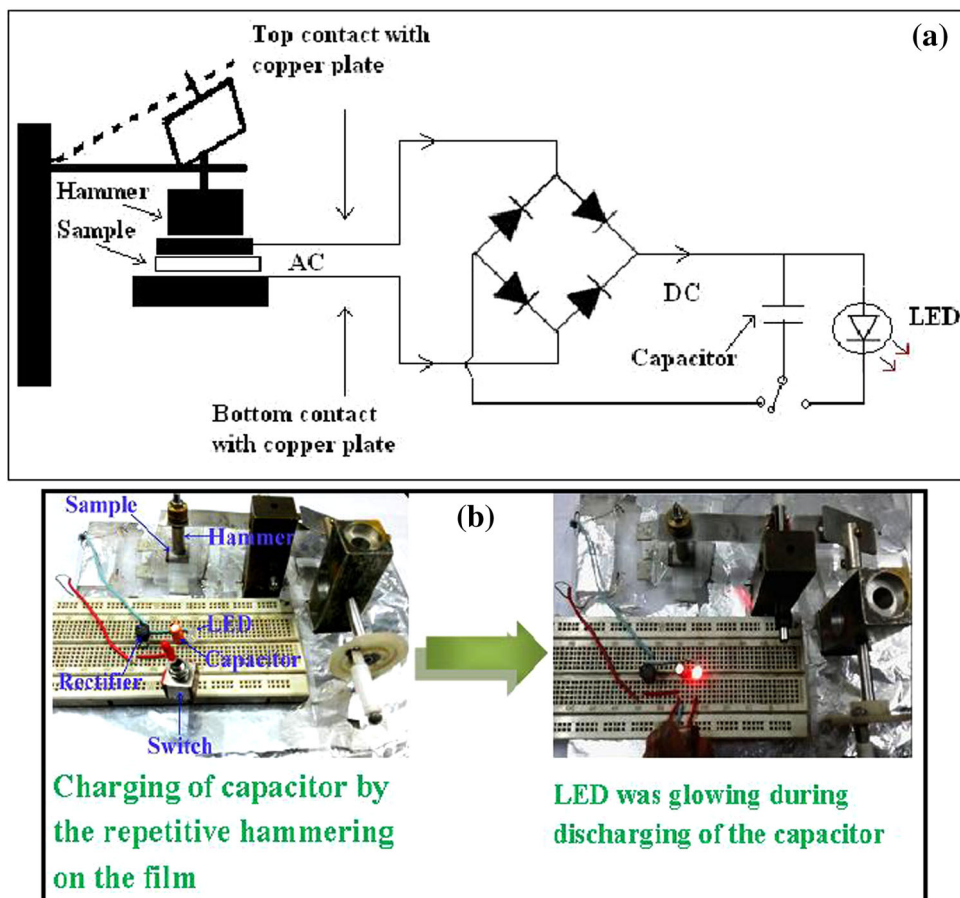
matrix for the poled sample (Fig. 6c). All the measurements were performed at a fixed strain generated by a fixed load. Nature of the oscillations generated by a single stroke of the hammer is depicted in Fig. 6d. One may observe a damped oscillating behavior in the output signal. The damped oscillation arising out of repetitive hammering appeared as a based-band in all the measurements shown in Fig. 5a, b. Similar behavior was observed for all the films containing different amounts of ZnO loading in PVDF matrix. The discharging of the capacitor is shown in Fig. 6e. The change in the output voltage with increased nano-ZnO loading is depicted graphically in Fig. 7b. One may observe an increase in the output voltage with increased nano-ZnO loading. This effect of increased inclusion of nano-ZnO filler in PVDF matrix will be better understood from the following discussion.

When the volume fraction of nano-ZnO is small, the semiconducting particles (nano-ZnO) would form small and isolated islands within the insulating matrix and naturally the conductivity would become activated. But, with increased volume fraction of the semiconducting material, the islands would become larger, numerous and comparable to the insulating medium separating the two adjacent nanocrystallites. This would culminate in the reduction in the activation energy. In the former case, the contribution to the electrical property would come from the percolation along the semiconducting maze and tunneling of electron between the isolated islands (semiconducting sites). With further decrease in the number density of ZnO nanocrystallites, i.e., the volume fraction of the filler, the density of percolation channels would get reduced. Now, as the electrical property would
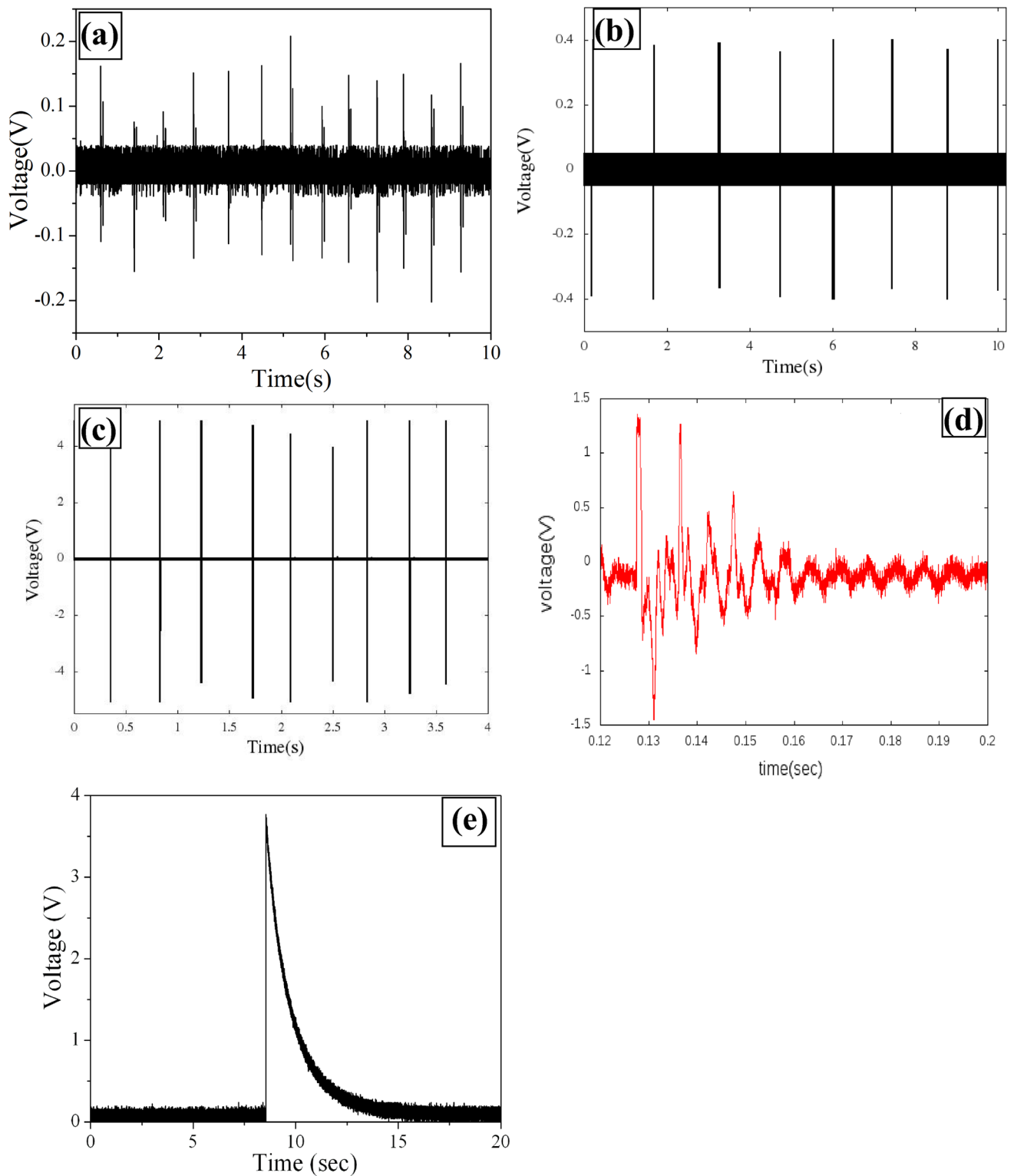
Fig. 6 Signal generated from a representative **a** pristine unpoled PVDF film, **b** PVDF film, **c** poled nano-ZnO/PVDF (0.2 M ZnO loading), **d** damped oscillation generated by a single hammer stroke, **e** discharging behavior of a capacitor (100 μF) used to light a *red* LED

depend on the density of percolation paths and the resistance offered by different paths, the conductivity would tend to decrease in these systems with the decrease in volume fraction of the ZnO nanocrystals. Thus, the nearly linear increase in output voltage will be limited by a critical filler (nano-ZnO) concentration

when the composite will lose the above property. Beyond the critical concentration of the filler, the composite will show the typical properties of nano-ZnO film. The composite material will tend to lose its flexibility faster once the critical concentration of the filler (ZnO nanocrystallites) is reached.

The change in output voltage with three different stress values for pristine PVDF and nano-ZnO/PVDF films is depicted in Fig. 7a. Variation of output voltage with ZnO loading in PVDF matrix at the above three different stress values imparted to the composite films is represented in Fig. 7b. The output voltage was highest for nano-ZnO/PVDF films having higher ZnO content. Open-circuit voltage ~ 4 V (peak to peak) was obtained. It may be stressed that the current was low due to high internal resistance of the nano-ZnO/PVDF composite film and maximum power was of the order of a few nanowatts. A capacitor (100 μF) was charged using a bridge rectifier (model no: B40C800) with the help of this nanogenerator and was discharged to light a red LED as per the nature of discharging behavior of the capacitor shown in Fig. 6e.

Now the piezoelectric charge coefficient, d_{ij}, is the polarization charge generated per unit of mechanical stress applied to a piezoelectric material and the piezoelectric voltage coefficient, g_{ij}, is the electric field generated by a piezoelectric material per unit of mechanical stress applied. The first subscript to d_{ij} and g_{ij} indicates the direction of polarization and electric field generated in the material. The second subscript is the direction of the applied stress. It may be noted here that the ZnO/PVDF film was held between two clamps and the film was stressed only in the vertically down direction. The film took a symmetric dimple type of shape. Since the induced polarization in this case is parallel to direction in which this piezoelement is polarized, the piezoelectric coefficient of interest will be d_{33} and g_{33} only. The piezoelectric charge coefficient (d_{33}) and piezoelectric voltage coefficient (g_{33}) were evaluated with the help of equations (Eqs. 7 and 8) for the pristine PVDF before and after inclusion of nano-ZnO in different proportions in the PVDF matrix (Fig. 7c, d) from the impedance and open-circuit piezoelectric voltage.

$$d_{33} = \frac{\text{induced polarization}}{\text{applied mechanical stress}} = \frac{\varepsilon_r \varepsilon_0 V}{tS} \tag{7}$$

$$g_{33} = \frac{\text{electrical field}}{\text{applied mechanical stress}} = \frac{V}{tS} \tag{8}$$

where t, V and S are the thickness of the film, voltage generated across the film and applied stress, respectively.

It was observed that the piezocoefficients of the PVDF flexible and free-standing films increased significantly with the inclusion of nano-ZnO in the PVDF matrix making the films conducive for nanogenerator application. Figure 7e, f shows the more or less linear variation of d_{33} and g_{33} with different stresses, respectively. Piezoelectric coefficient of PVDF is generally ~ 20–28 pC/N [24, 25], while that for ZnO is ~ 12.3 pC/N [26]. The composites made out of the two showed significant increase in the value of piezocoefficient. Similar modulation of the piezocoefficient in composites was reported in Ref. [25].

In pursuit of increasing the capability of delivering higher current, obvious choice was to decrease the resistance of the ZnO/PVDF films. This could be attained either by increasing the nano-ZnO loading or by the inclusion of metal-doped ZnO. In the first case, we observed that with the increase of nano-ZnO loading in PVDF matrix the flexibility of the films decreased. The films became sticky and were no more free-standing in nature. For the second case, inclusion of metal-doped ZnO, the dielectric constant decreased significantly due to increased conductivity of the doped ZnO. This resulted in lowering the capacity of holding the charges with applied stress. The piezocoefficients of the films also became low. Thus, a happy compromise was made to attain a critical load of nano-ZnO in PVDF matrix to attain the best value of dielectric constant and piezocoefficient such that an acceptable level of power generated by the ZnO/PVDF nanogenerator with acceptable flexibility and free-standing nature could be attained.

4 Conclusions

Free-standing flexible composite films of nano-ZnO/PVDF were deposited by sol–gel technique. These films were subjected to energy harvesting studies. It was observed that the output voltage increased (nearly doubled) upon poling for pristine PVDF films and increased 10 times with the inclusion of nano-ZnO in the PVDF matrix for poled samples. The output voltage was highest for nano-ZnO/PVDF films having higher ZnO content. Open-circuit AC voltage ~ 4 V was obtained. It may be stressed that the current was low due to high internal resistance of the nano-ZnO/PVDF composite film and maximum power was few nanowatt. The output voltage could be stored using a bridge rectifier and a capacitor. A happy compromise was made on the critical loading of nano-ZnO filler in PVDF matrix to attain the best value of dielectric constant and piezocoefficient such that an acceptable level of power generated by the ZnO/PVDF nanogenerator could be attained. This study reported a faithful and reproducible route of obtaining ZnO/PVDF nanogenerator with improved performance for energy harvesting applications.
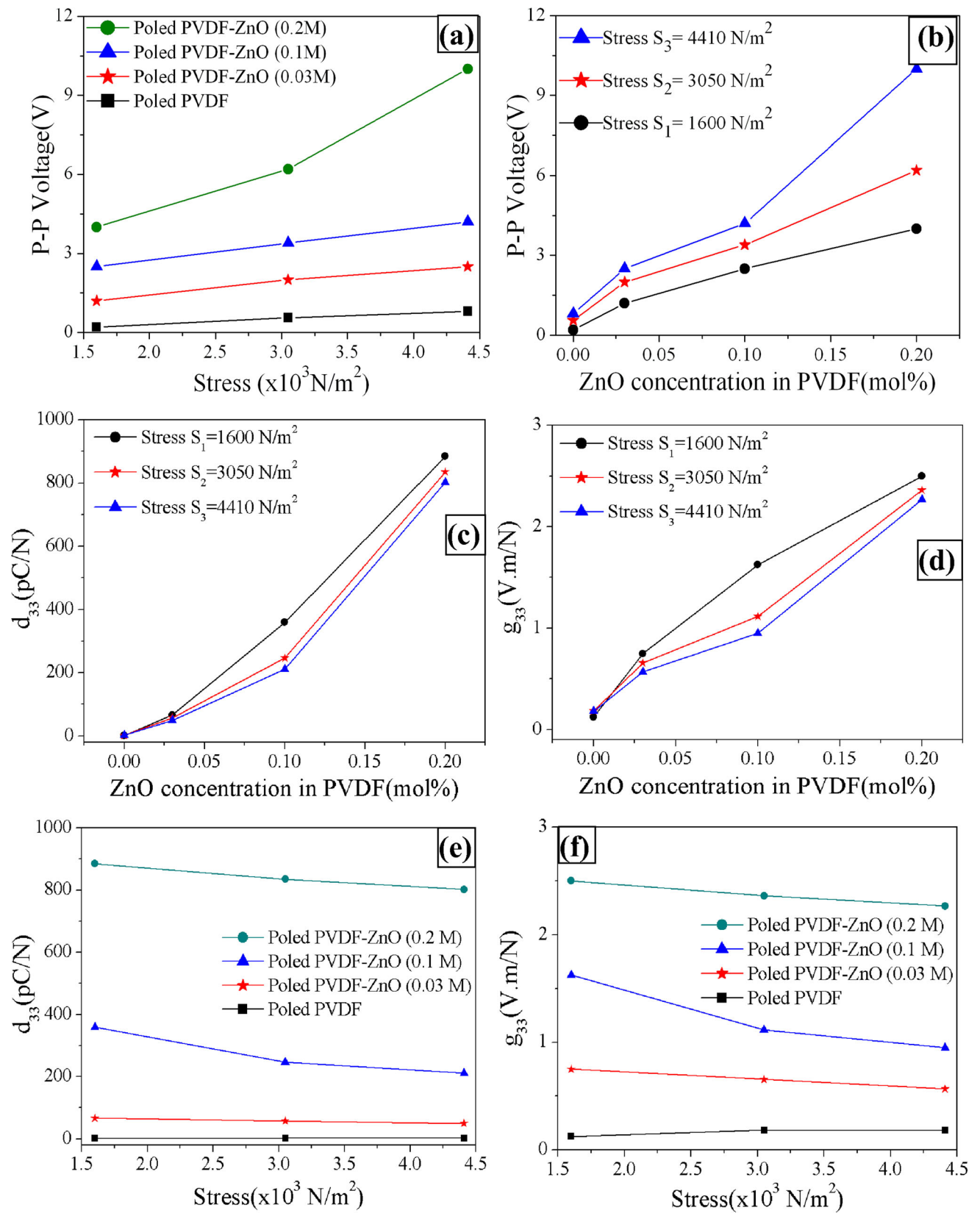
◀**Fig. 7** Variation of output voltage: **a** with three different stresses for nano-ZnO/PVDF for different ZnO loadings along with that for poled pristine PVDF film and **b** with ZnO loading in PVDF matrix measured at different stresses imparted to the composite films. Variation of piezoelectric charge coefficient (d_{33}) with: **c** different ZnO loadings in PVDF matrix and for pristine PVDF and **d** different stresses

The films being flexible and free-standing will have an edge over other NG materials used so far.

References

1. K.H. Kim, B. Kumar, K.Y. Lee, H.K. Park, J.H. Lee, H.H. Lee, H. Jun, D. Lee, S.W. Kim, Piezoelectric two-dimensional nanosheets/anionic layer heterojunction for efficient direct current power generation. Sci. Rep. **3**, 1–6 (2017)

2. L. Chen, X. Xu, P. Zeng, J. Ma, Integration of energy harvester for self-powered wireless sensor network nodes. Int. J. Distrib. Sens. Netw. **2014**, 1–7 (2014)

3. T. Huang, C. Wang, H. Yu, H. Wang, Q. Zhang, M. Zhu, Human walking-driven wearable all-fiber triboelectric nanogenerator containing electrospun polyvinylidene fluoride piezoelectric nanofibers. Nano Energy **14**, 226–235 (2015)

4. K.-I. Park, S. Xu, Y. Liu, G.-T. Hwang, S.-J.L. Kang, Z.L. Wang, K.J. Lee, Piezoelectric BaTiO₃ thin film nanogenerator on plastic substrates. Nano Lett. **10**(12), 4939–4943 (2010)

5. Z.-H. Lin, Y. Yang, J.M. Wu, Y. Liu, F. Zhang, Z.L. Wang, BaTiO₃ nanotubes-based flexible and transparent nanogenerators. J. Phys. Chem. Lett. **3**, 3599–3604 (2012)

6. G. Zhu, R. Yang, S. Wang, Z.L. Wang, Flexible high-output nanogenerator based on lateral ZnO nanowire array. Nano Lett. **10**, 3151–3155 (2010)

7. K.Y. Lee, M.K. Gupta, S.W. Kim, Transparent flexible stretchable piezoelectric and triboelectric nanogenerators for powering portable electronics. Nano Energy **14**, 139–160 (2014)

8. Y.K.A. Low, L.Y. Tan, L.P. Tan, F.Y.C. Boey, K.W. Ng, Increasing solvent polarity and addition of salts promote β-phase poly(vinylidene fluoride) formation. J. Appl. Polym. Sci. **128**, 2902–2910 (2013)

9. V. Strashilov, G. Alexieva, B. Vincent, V.S. Nguyen, D. Rouxel, Structural impact on piezoelectricity in PVDF and P(VDF-TrFE) thin films. Appl. Phys. A **118**, 1469–1477 (2015)

10. Y.-J. Lee, J. Wang, S.R. Cheng, J.W.P. Hsu, Solution processed ZnO hybrid nanocomposite with tailored work function for improved electron transport layer in organic photovoltaic devices. ACS Appl. Mater. Interfaces **5**, 9128–9133 (2013)

11. W.K. Choi, D.H. Park, B.W. Kwon, D.I. Son, US Patent No. WO2012165753 A1, Application No. PCT/KR2012/001433 (2012)

12. C.J.L. Constantino, A.E. Job, R.D. Simoes, J.A. Giacometti, V. Zucolotto, O.N. Oliveira Jr., G. Gozzi, D.L. Chinaglia, Phase transition in poly(vinylidene fluoride) investigated with micro-Raman spectroscopy. Appl. Spectrosc. **59**, 275–279 (2005)

13. S. Satapathy, S. Pawar, P.K. Gupta, K.B.R. Varma, Effect of annealing on phase transition in poly(vinylidene fluoride) films prepared using polar solvent. Bull. Mater. Sci. **34**, 727–733 (2011)

14. T. Boccaccio, A. Bottino, G. Capannelli, P. Piaggio, Characterization of PVDF membranes by vibrational spectroscopy. J. Membr. Sci. **210**, 315–329 (2002)

15. Y. Bormashenko, R. Pogreb, O. Stanevsky, E. Bormashenko, Vibrational spectrum of PVDF and its interpretation. Polym. Testing **23**, 791–796 (2004)

16. B. Mattsson, H. Ericson, L.M. Torell, F. Sundholm, Degradation of a fuel cell membrane, as revealed by micro-Raman spectroscopy. Electrochim. Acta **45**, 1405–1408 (2000)

17. B. Mattsson, H. Ericson, L.M. Torell, F. Sundholm, Micro-Raman investigations of PVDF-based proton-conducting membranes. J. Polym. Sci. A Polym. Chem. **37**, 3317–3327 (1999)

18. M.T. Riosbaas, K.J. Loh, G.O. Bryan, B.R. Loyol, In situ phase change characterization of PVDF thin films using Raman spectroscopy. Proc. SPIE **9061**, 90610Z (2014). doi:10.1117/12.2045430

19. A. Kaschner, U. Haboeck, M. Strassburg, M. Strassburg, G. Kaczmarczyk, A. Hoffmann, C. Thomsen, A. Zeuner, H.R. Alves, D.M. Hofmann, B.K. Meyer, Nitrogen-related local vibrational modes in ZnO:N. Appl. Phys. Lett. **80**, 1909–1911 (2002)

20. B. Cheng, Y. Xiao, G. Wu, L. Zhang, The vibrational properties of one-dimensional ZnO: Ce nanostructures. Appl. Phys. Lett. **84**, 416–418 (2004)

21. C. Bundesmann, N. Ashkenov, M. Schubert, D. Spemann, T. Butz, E.M. Kaidashev, M. Lorenz, M. Grundmann, Raman scattering in ZnO thin films doped with Fe, Sb, Al, Ga, and Li. Appl. Phys. Lett. **83**, 1974–1976 (2003)

22. J. Bird, *Electrical Circuit Theory and Technology* (Routledge, Abingdon, 2014), p. 567

23. A.R. West, D.C. Sinclair, N. Hirose, Characterization of electrical materials, especially ferroelectrics, by impedance spectroscopy. J. Electroceram. **1**, 65–71 (1997)

24. J.S. Harrison, Z. Ounaies, *Piezoelectric Polymers Encyclopedia of Polymer Science and Technology* (Wiley, New York, 2002), pp. 474–498

25. K.S. Ramadan, D. Sameoto, S. Evoy, A review of piezoelectric polymers as functional materials for electromechanical transducers. Smart Mater. Struct. **23**, 033001 (2014)

26. H. Landolt, R. Börnstein, H. Fischer, O. Madelung, G. Deuschle, *Landolt-Bornstein: Numerical Data and Functional Relationships in Science and Technology*, ed. by O. Madelung. New Series, Group III, Vol. 17 (Springer-Verlag, Berlin, 1987), p. 164